Neurosci. Bull. October, 2019, 35(5):781–790
https://doi.org/10.1007/s12264-019-00397-2

www.neurosci.cn
www.springer.com/12264

ORIGINAL ARTICLE

Brain-wide Mapping of Mono-synaptic Afferents to Different Cell Types in the Laterodorsal Tegmentum

Xiaomeng Wang[1] · Hongbin Yang[1] · Libiao Pan[1] · Sijia Hao[1] · Xiaotong Wu[1] · Li Zhan[1] · Yijun Liu[1] · Fan Meng[1] · Huifang Lou[1] · Ying Shen[1] · Shumin Duan[1] · Hao Wang[1]

Received: 29 December 2018 / Accepted: 16 February 2019 / Published online: 5 June 2019

Abstract The laterodorsal tegmentum (LDT) is a brain structure involved in distinct behaviors including arousal, reward, and innate fear. How environmental stimuli and top-down control from high-order sensory and limbic cortical areas converge and coordinate in this region to modulate diverse behavioral outputs remains unclear. Using a modified rabies virus, we applied monosynaptic retrograde tracing to the whole brain to examine the LDT cell type specific upstream nuclei. The LDT received very strong midbrain and hindbrain afferents and moderate cortical and hypothalamic innervation but weak connections to the thalamus. The main projection neurons from cortical areas were restricted to the limbic lobe, including the ventral orbital cortex (VO), prelimbic, and cingulate cortices. Although different cell populations received qualitatively similar inputs, primarily *via* afferents from the periaqueductal gray area, superior colliculus, and the LDT itself, parvalbumin-positive (PV^+) GABAergic cells received preferential projections from local LDT neurons. With regard to the different subtypes of GABAergic cells, a considerable number of nuclei, including those of the ventral tegmental area, central amygdaloid nucleus, and VO, made significantly greater inputs to somatostatin-positive cells than to PV^+ cells. Diverse inputs to the LDT on a system-wide level were revealed.

Keywords Laterodorsal tegmentum · Rabies virus retrograde tracing · Limbic lobe · Mice

Introduction

The laterodorsal tegmentum (LDT), a nucleus located in the brainstem, has been found to play critical roles in diverse behaviors including arousal, reward, and innate defense [1–7]. Neurotransmitter identity studies have revealed that neurons in the LDT are arranged into a highly heterogeneous structure which includes cholinergic, glutamatergic, and GABAergic neurons [8, 9]. Although the co-expression of cholinergic and glutamatergic cells was initially suggested [8], a more recent study has shown that they represent two separate populations of neurons [9]. Interestingly, different cell types in the LDT have been implicated in distinct brain functions. For decades, the cholinergic cells in the LDT have received much attention since these, together with cholinergic cells in the pedunculopontine tegmentum and basal forebrain, make up the major cholinergic projection system in the central nervous system [10]. Cholinergic LDT cells send extensive ascending projections to the forebrain, including the thalamus, basal forebrain, and cerebral cortex [11, 12]. The LDT has been proposed as the key nodal structure in arousal. Recent studies have shown that all cholinergic LDT cells are maximally active during the waking period and during rapid-eye-movement (REM) sleep [13]. The optogenetic

Xiaomeng Wang, Hongbin Yang and Libiao Pan have contributed equally to this work.

Electronic supplementary material The online version of this article (https://doi.org/10.1007/s12264-019-00397-2) contains supplementary material, which is available to authorized users.

✉ Hao Wang
haowang@zju.edu.cn

[1] Department of Neurobiology and Department of Neurosurgery of The Second Affiliated Hospital, Key Laboratory of Medical Neurobiology of the Ministry of Health of China, NHC and CAMS Key Laboratory of Medical Neurobiology, Zhejiang University School of Medicine, Hangzhou 310058, China

activation of cholinergic neurons in the LDT during non-REM sleep is able to induce an increase in REM sleep episodes [6]. In addition to its role in sleep regulation, many reports have focused on the activity of the LDT in regulating the firing pattern of dopaminergic cells in the ventral tegmental area (VTA) [1, 3], and thus its involvement in dopamine-related reward learning. Similarly, involvement of the LDT in drug addiction, including nicotine and amphetamine, has also been implied [2, 14, 15], presumably through its cholinergic and/or glutamatergic projection to the VTA [16–19]. Further studies using optogenetics have shown that the excitation of either cholinergic inputs or glutamatergic projections from the LDT to the VTA is capable of mediating reward [19, 20]. Our own laboratory recently uncovered a further crucial role of GABAergic LDT cells in innate defensive behaviors induced by olfactory cues. In this study, the optogenetic activation of parvalbumin-positive (PV^+) GABAergic LDT cells induces an immediate fear response in naïve mice, whereas photo-activation of somatostatin-positive (SOM^+) GABAergic cells suppresses any fear response induced by the presence of a predator odor [7]. Overall, with these strong associations of the LDT with behaviors, it is still puzzling how the different LDT cell subtypes are capable of coordinating so many diverse behaviors, especially those like reward and aversion which appear to be at opposite poles. In addition, the brain areas associated with higher-order functions, including the sensory and prefrontal cortical areas may also be involved in the regulation of those basic innate behaviors through their projections to the LDT, acting *via* a top-down mechanism. Therefore, any attempt to map the inputs from the whole brain to a specific cell type in the LDT would likely yield results of strong interest and broad application.

Although previous studies have explored the afferent and efferent projections of the LDT [21, 22], the lack of consideration of cell-type specificity in these studies has limited their implications. By using a modified rabies virus, here we explore the brain-wide monosynaptic inputs to the LDT, tracing local and long-range inputs to four genetically-defined LDT cell types (glutamatergic, cholinergic, and PV^+ and SOM^+ GABAergic cells) and generate a map of whole-brain monosynaptic inputs to the LDT. Our study aids in the understanding of how the LDT coordinates such a breadth of distinctive behaviors.

Materials and Methods

Animals

All animal experiments were performed according to the Guidelines for the Care and Use of Laboratory Animals of Zhejiang University. The protocol was approved by the Zhejiang University animal experimentation committee. *CHAT-IRES-Cre*, *VGLUT2-IRES-Cre, PV-IRES-Cre*, and *SST-IRES-Cre* mice were obtained from the Jackson Laboratory. *C57BL/6J* mice were obtained from the Shanghai Laboratory Animal Center, Chinese Academy of Sciences. Male Cre mice (4/group) or female *C57BL/6J* mice ($n = 3$) at the age of 2–6 months were used in the experiments and given food and water *ad libitum*, at (22 ± 1) °C and 55% ± 5% humidity.

Virus and Viral Injection

All the viruses used in the trans-synaptic retrograde tracing experiments: AAV-CAG-Dio-RG (AAV2/9, 6.8×10^{12} genomic copies/mL), AAV-CAG-Dio-TVA-eGFP (AAV2/9, 6.8×10^{12} genomic copies/mL) and RV-EvnA-DsRed RV (5.0×10^8 genomic copies/mL), were provided by Professor Fuqiang Xu (Wuhan, China). Viral injections were performed as described previously [7]. In brief, mice were deeply anesthetized with sodium pentobarbital (1% wt/vol) and placed in a stereotactic apparatus (David Kopf Instruments, Tujunga, CA). A 100-nL mixture of AAV-CAG-Dio-TVA-eGFP and AAV-CAG-Dio-RG (1:1) was infused unilaterally into the LDT (AP –5.2, ML –0.4, DV –3.7 mm relative to Bregma) on day 1. After 3 weeks to allow helper viruses become well expressed, the mice received a second surgery in which 300 nL of RV-EvnA-DsRed was injected into the same location. One week after injecting the rabies virus, the mice were sacrificed for fluorescence imaging and analysis. In control experiments, the same volume virus and experimental strategy were used in wild-type (*C57BL/6J*) mice.

Tissue Preparation and Fluorescence Imaging

Mice were deeply anesthetized with sodium pentobarbital (1% wt/vol) and perfused with saline followed by 4% paraformaldehyde (wt/vol) in 0.1 mol/L phosphate-buffered saline (PBS). Brain samples were post-fixed in the same paraformaldehyde solution for 6–8 h at 4 °C, then transferred to 30% sucrose (wt/vol) in 0.1 mol/L PBS over night; then, 40-μm coronal cryo-sections were cut on a cryo-microtome (Leica CM1900). After staining with the nuclear dye DAPI, the sections were used for imaging. Confocal images were captured under a 10× or 20× objective (Olympus FV-1200).

Cell Counts and Statistics

For the qualification of starter cells and afferent input cells, we sampled every fourth 40-μm section from + 2.5 to − 5.5 mm from bregma, according to the reference atlas

(the Allen Mouse Brain Atlas) and counted the cells manually and blindly using ImageJ software. For statistical tests, all values are presented as the mean ± SEM. A Kruskal-Wallis test or one-way ANOVA was used for group differences as appropriate and Dunn's *post hoc* test or Tukey's *post hoc* test was used for multiple comparisons, all using GraphPad Prism 6. Differences were considered statistically significant when $P < 0.05$. For details of the statistical analysis for each figure, see Table S1.

Results

Experimental Strategy

In order to make a cell type specific whole-brain map of inputs to the LDT, four Cre mouse lines were used to target different subpopulations of LDT neurons: *CHAT-IRES-Cre* for cholinergic neurons, *VGLUT2-IRES-Cre* for glutamatergic neurons, and *PV-IRES-Cre* and *SST-IRES-Cre* for the two subtypes of GABAergic neurons. The experimental strategies are shown in Fig. 1A. Briefly, we used a modified rabies virus [23, 24] in combination with two Cre-dependent helper viruses (AAV-CAG-Dio-TVA-eGFP and AAV-CAG-Dio-RG). The modified rabies virus (RV) could not achieve trans-synaptic transport by itself because of the lack of the RV- glycoprotein. On day 1, a 100 nL mixture of two kinds of adeno-associated virus (AAV) expressing target proteins in a Cre-dependent manner, was injected into the LDT. After 3 weeks, the modified rabies virus RV-EvnA-DsRed was injected into the same site. Under the cre/loxp system, with ligand/receptor and RV-G control, we were able to label presynaptic inputs in a monosynaptic manner with cell-type specificity. One week after injection of the rabies virus, the mice were sacrificed and whole-brain sections were cut for fluorescence imaging (Fig. 1A, B).

We also injected two Cre-dependent helper viruses (AAV-CAG-Dio-TVA-eGFP and AAV-CAG-Dio-RG) and the modified rabies virus into the LDT of wild-type mice ($n = 3$) to test any leakage of this virus tracing system (Fig. S1A). In the control experiment, we found that although very little red cell debris was observed, there was no neuronal labeling of either TVA-eGFP or RV-DsRed fluorescence protein in the LDT (Fig. S1B). This result indicated that our virus tracing system worked well with little leakage.

Identification of the Major Long-Range Inputs to the LDT

To define the boundaries of different nuclei, each section was labeled by DAPI, a fluorescent nuclear stain. Presynaptic inputs labeled with DsRed were identified manually throughout the rostro-caudal axis of the brain according to the reference atlas registering their locations. After taking all the factors into account, we sampled every fourth 40-μm section from + 2.5 to − 5.5 from bregma. We injected the virus into 5–6 mice from each Cre line. In all cases, only mice in which starter cells were restricted to the LDT were counted (Figs. 2A, 3A, 4A, and 5A, $n = 4$/group).

We then calculated the convergence index (ratio between the whole-brain input cell count and the starter cell number) for each case. We found that each subtype of cell in the LDT seemed to receive comparable inputs per starter cell (Fig. 1C). Next, we examined the input intensity of individual nucleus for each LDT cell type. We provided details of afferent nuclei (Fig. S2), noting any afferent intensity > 1% (determined by dividing the input cell count within an individual nucleus by all the input cell counts throughout the whole brain) for glutamatergic (Fig. 2B, C), cholinergic (Fig. 3B, C), PV^+-GABAergic (Fig. 4B, C), and SOM^+-GABAergic Fig. 5B, C) LDT cells. Many upstream nuclei with afferent intensities < 1% were also traced. These are listed in the spreadsheets of Fig. S3.

Next, we dissected the whole brain into 5 functional areas and calculated the afferent intensity of each area to the LDT with cell-type specificity (Fig. 6). We found that most of the afferents to the LDT originated from the midbrain and hindbrain, and slight but measurable differences between the four cell types were only observed in the hindbrain ($P = 0.023$). The hypothalamus and the cortex also made moderate connections with LDT neurons with clear cell-type preference ($P < 0.0001$ and $P = 0.006$, respectively). The hypothalamus, for example, displayed a clear preference for SOM^+ and $VgluT2^+$ neurons. Very few direct projections to the LDT were received from the thalamus.

Identification of the Detailed Cortical Inputs to the LDT

We then analyzed the detailed cortical inputs to the LDT. It is very interesting to note that although cortical areas only made moderate direct projections to the LDT, they showed unique patterns. For example, among the different cell subtypes, $VGluT2^+$ neurons received much stronger innervation from several cortical areas including the motor cortex ($P = 0.027$), ventral orbital cortex ($P = 0.0003$), cingulate cortex ($P = 0.0169$), medial orbital cortex ($P = 0.0215$), and agranular insular cortex ($P = 0.0173$) (Fig. 7A). These results suggest that the cortical areas prefer to innervate glutamatergic cells in the LDT. In addition, none of the sensory cortical areas directly innervated the LDT, with the exception of the somatosensory cortex which sent very low-level inputs to the LDT.

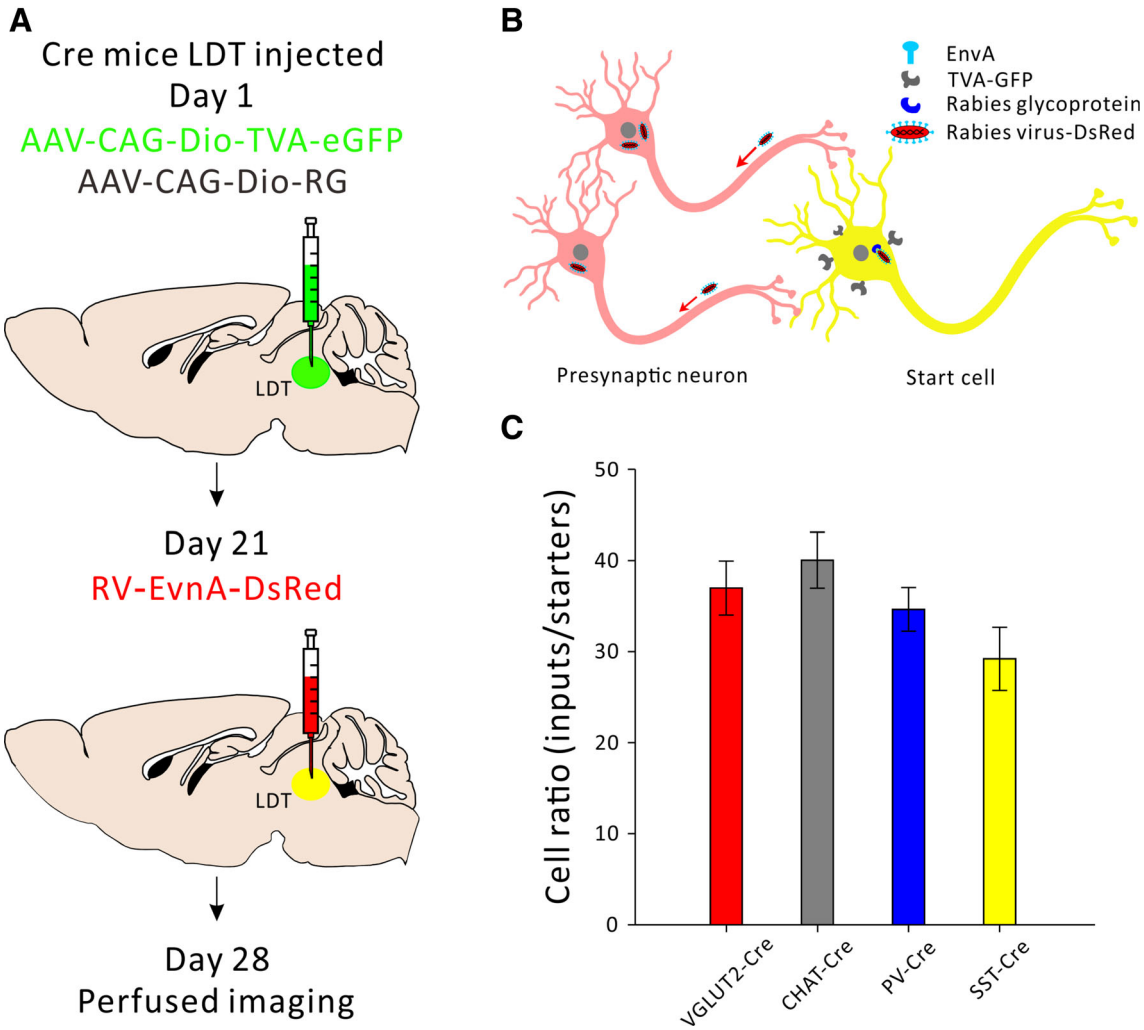

Fig. 1 Schematic of the experimental strategy. **A** Timeline of virus injection into the LDT for retrograde trans-synaptic tracing. **B** Schematic of cell-type specific circuit tracing. The AAV-CAG-Dio-TVA-eGFP virus (AAV2/9) and the AAV-CAG-Dio-RG (AAV2/9) virus are Cre-dependent. RV-EvnA-DsRed only infects TVA-expressing cells and spreads to the primary afferent cells with the help of the glycoprotein. **C** Ratios of all the input cell counts from the whole brain to starter cell counts in the LDT ($n = 4$, $P = 0.106$, mean ± SEM).

Among the different cortical areas, most of the projection cells originated from the motor cortex and the limbic cortical areas, including the ventral orbital, prelimbic, and cingulate cortices (Fig. 7A). There were also a few cortical regions, such as the somatosensory, retrosplenial, lateral orbital, parietal association, medial orbital, and agranular insular cortices that provided very weak innervation (< 1% of total inputs) to the LDT (Fig. 7A). The distribution of input strength is shown in Fig. 7B.

Comparison of Inputs Between Different Cell Types

When we calculated the afferent intensity among the different brain areas, we found that the superior colliculus, lateral hypothalamic (LH) area, periaqueductal gray area, and substantia nigra contained more primary input neurons than most of the other labeled nuclei. Interestingly, a few neighboring nuclei of these densely-labeled nuclei (e.g. the ventromedial hypothalamic nucleus, which is very close to the LH) showed more sparse labeling, indicating a high degree of spatial specificity for these long-range inputs. We also found that, although quite a few nuclei only sent innervation to two or three cell types, quantitative differences among the distributions of the primary input neurons to different cell types were detectable. For example, the afferent intensity of the central amygdala projection to the SOM^+ LDT neurons was significantly stronger than to the other three cell types ($P = 0.007$). In a similar manner, the afferent connections made by the LH to glutamatergic LDT neurons were also far more numerous than its connections to the other three cell types ($P < 0.0001$).

In order to understand the qualitative and quantitative differences in the input distributions among different cell

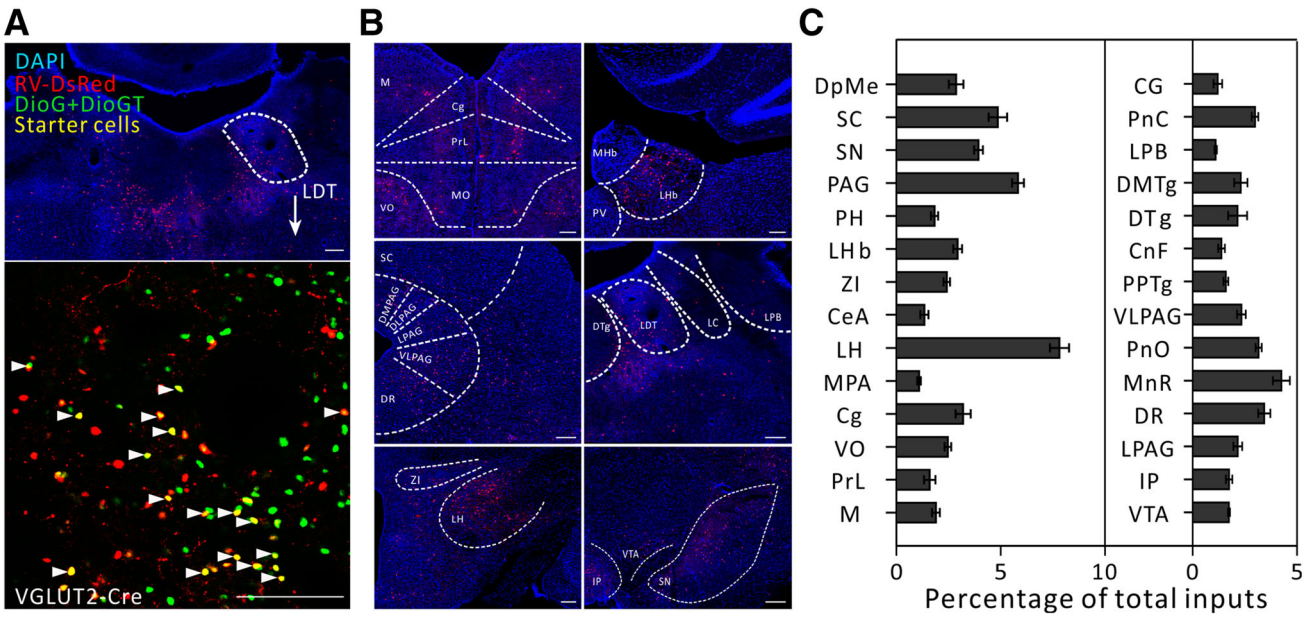

Fig. 2 Major long-range inputs to glutamatergic LDT neurons. **A** Representative confocal images of RV-labeled LDT neurons (red) in VGLUT2-IRES-Cre mice (upper panel) and starter cells restricted to the LDT (lower panel). As the starter cells express both eGFP and DsRed fluorescent proteins, they are shown in yellow (arrowheads). Scale bars, 150 μm. **B** Representative images of RV-labeled input neurons to glutamatergic LDT cells from selected brain regions. Scale bars, 150 μm. **C** Whole-brain distributions of afferent intensity to glutamatergic LDT cells. To measure the afferent intensity, we calculated the fraction input cell counts of specific brain region/whole brain input cell counts (n = 4, mean ± SEM).

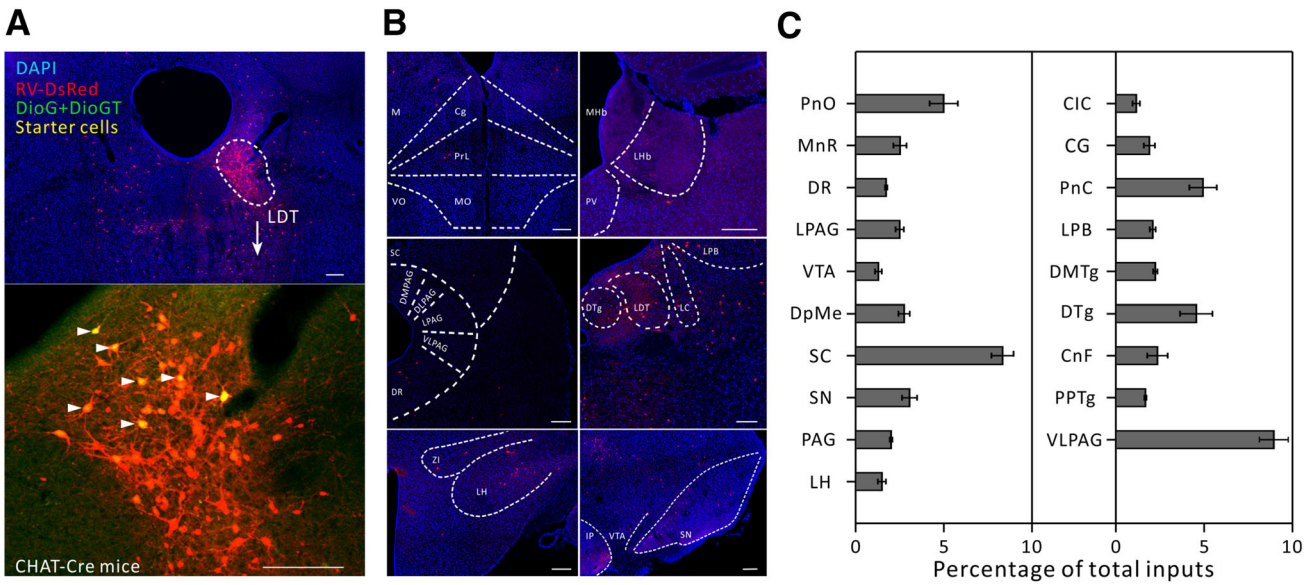

Fig. 3 Major long-range inputs to cholinergic LDT neurons. **A** Representative confocal images of RV-labeled LDT neurons (red) in CHAT-IRES-CRE mice (upper panel) and starter cells (yellow, arrowheads) restricted to the LDT (lower panel). Scale bars, 150 μm. **B** Representative images of RV-labeled input neurons to cholinergic LDT neurons from selected brain regions. Scale bars, 150 μm. **C** Whole-brain distributions of afferent intensity to cholinergic LDT neurons (n = 4, mean ± SEM).

types, we compared the afferent intensity of upstream nuclei one by one between glutamatergic and cholinergic cells (Fig. 8A), and PV^+ and SOM^+ GABAergic cells (Fig. 8B). We found that the ventral orbital cortex only made afferent connections to glutamatergic cells, having almost no connections to cholinergic cells in the LDT. For GABAergic cells in the LDT, SOM^+ neurons received far more inputs (> 3-fold) from several nuclei that belong to the limbic system, such as the VTA, central amygdala, and ventral orbital cortex, than did the PV^+ neurons.

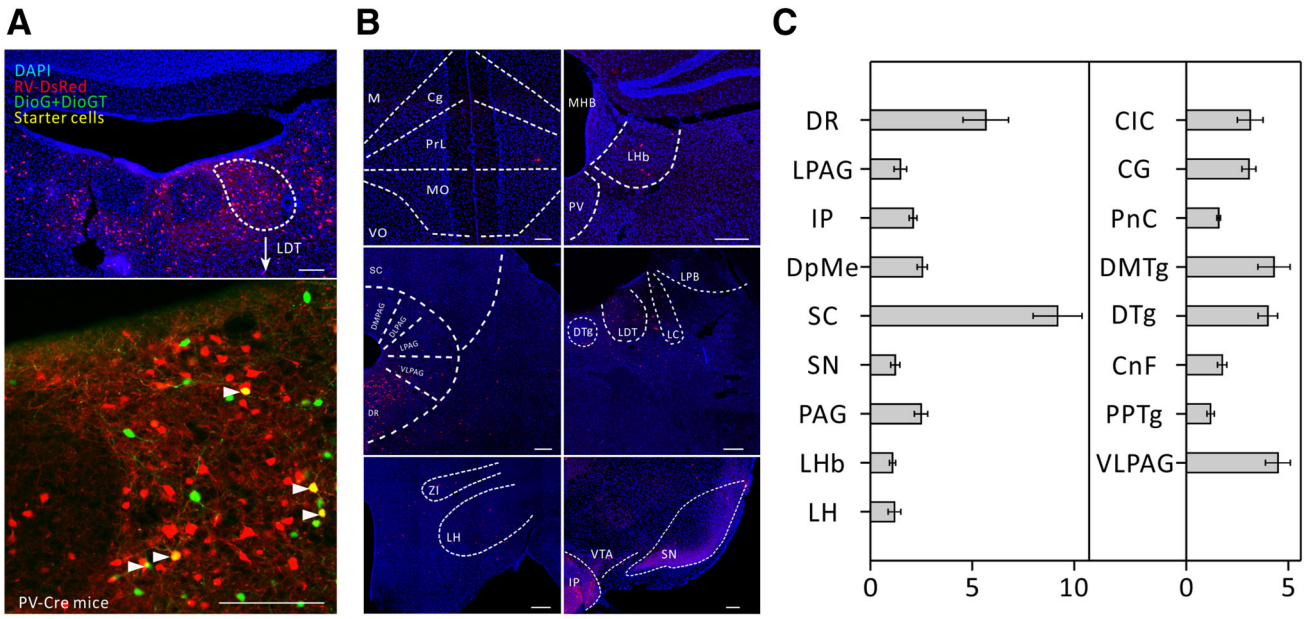

Fig. 4 Major long-range inputs to parvalbumin (PV)-positive LDT interneurons. **A** Representative confocal images of RV-labeled LDT neurons (red) in PV-IRES-Cre mice (upper panel) and starter cells (yellow, arrowheads) restricted to the LDT (lower panel). Scale bars, 150 μm. **B** Representative images of RV-labeled input neurons to PV-positive LDT interneurons from selected brain regions. Scale bars, 150 μm. **C** Whole-brain distributions of afferent intensity to PV-positive LDT interneurons (n = 4, mean ± SEM).

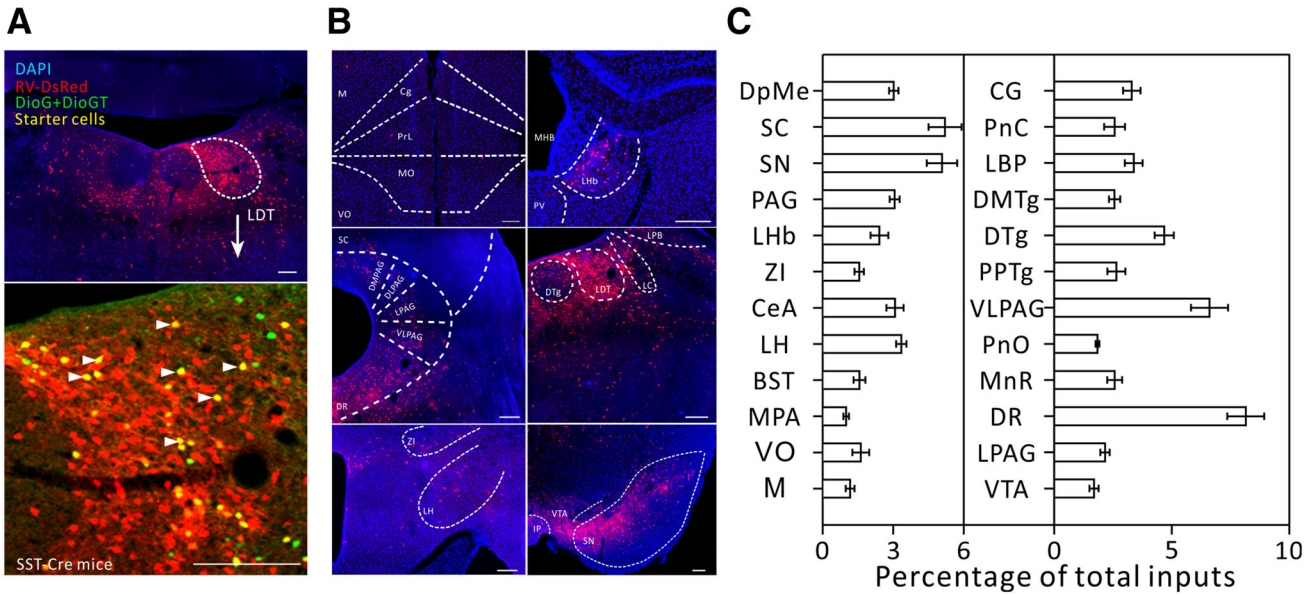

Fig. 5 Major long-range inputs to somatostatin (SOM)-positive LDT interneurons. **A** Representative confocal images of RV-labeled LDT neurons (red) in SST- IRES-Cre mice (upper panel) and starter cells (yellow, arrowheads) restricted to the LDT (lower panel). Scale bars, 150 μm. **B** Representative images of RV-labeled input neurons to SOM-positive LDT interneurons from selected brain regions. Scale bars, 150 μm. **C** Whole-brain distributions of afferent intensity to SOM-positive LDT interneurons (n = 4, mean ± SEM).

Identification Local Inputs to the LDT

It is important to note that all cell types in the LDT received very strong local innervation (Figs 8C, D), and this was particularly evident for PV^+ GABAergic cells. The afferent intensity of the LDT was 17.86% ± 0.20% for cholinergic, 9.11% ± 1.35% for glutamatergic, 27.77% ± 2.04% for PV^+-GABAergic, and 15.01% ± 1.62% for SOM^+-GABAergic cells (P = 0.0024, Fig. 8C). According to a previous study, there may be an extremely low level of TVA:GFP (avian-specific retroviral receptor:green fluorescent protein) expression in non-Cre-expressing cells. So

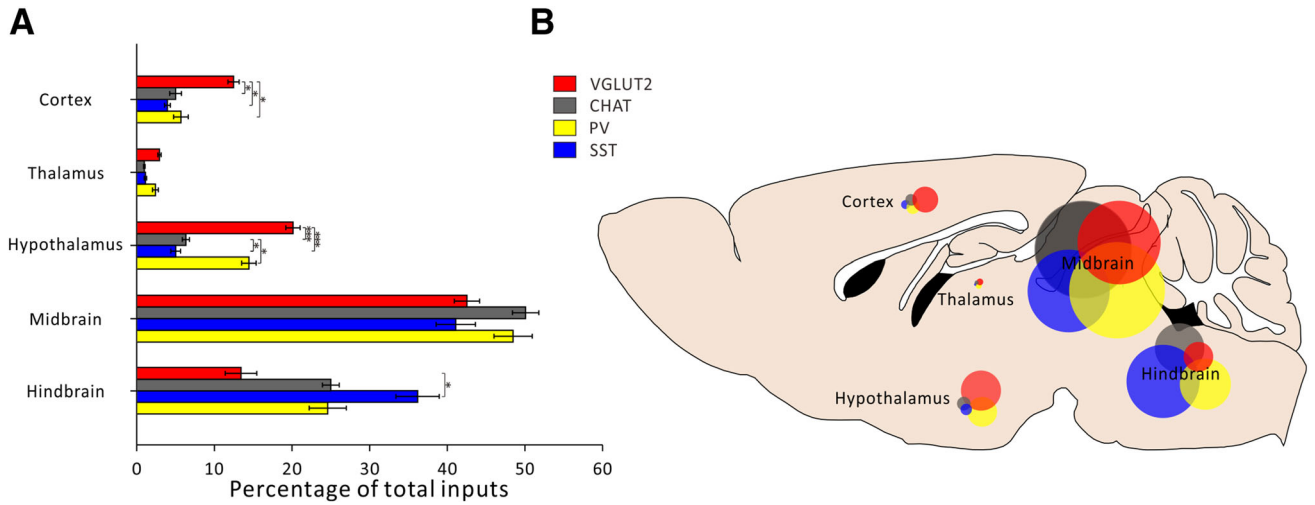

Fig. 6 Inputs to specific LDT cell types from selected brain regions. **A** Percentage of total inputs per selected brain region for specific LDT cell types ($n = 4$, $^*P < 0.05$, $^{***}P < 0.001$, mean ± SEM). **B** Schematic of afferent intensity of selected brain regions representing the percentages of total inputs per region for each LDT cell type.

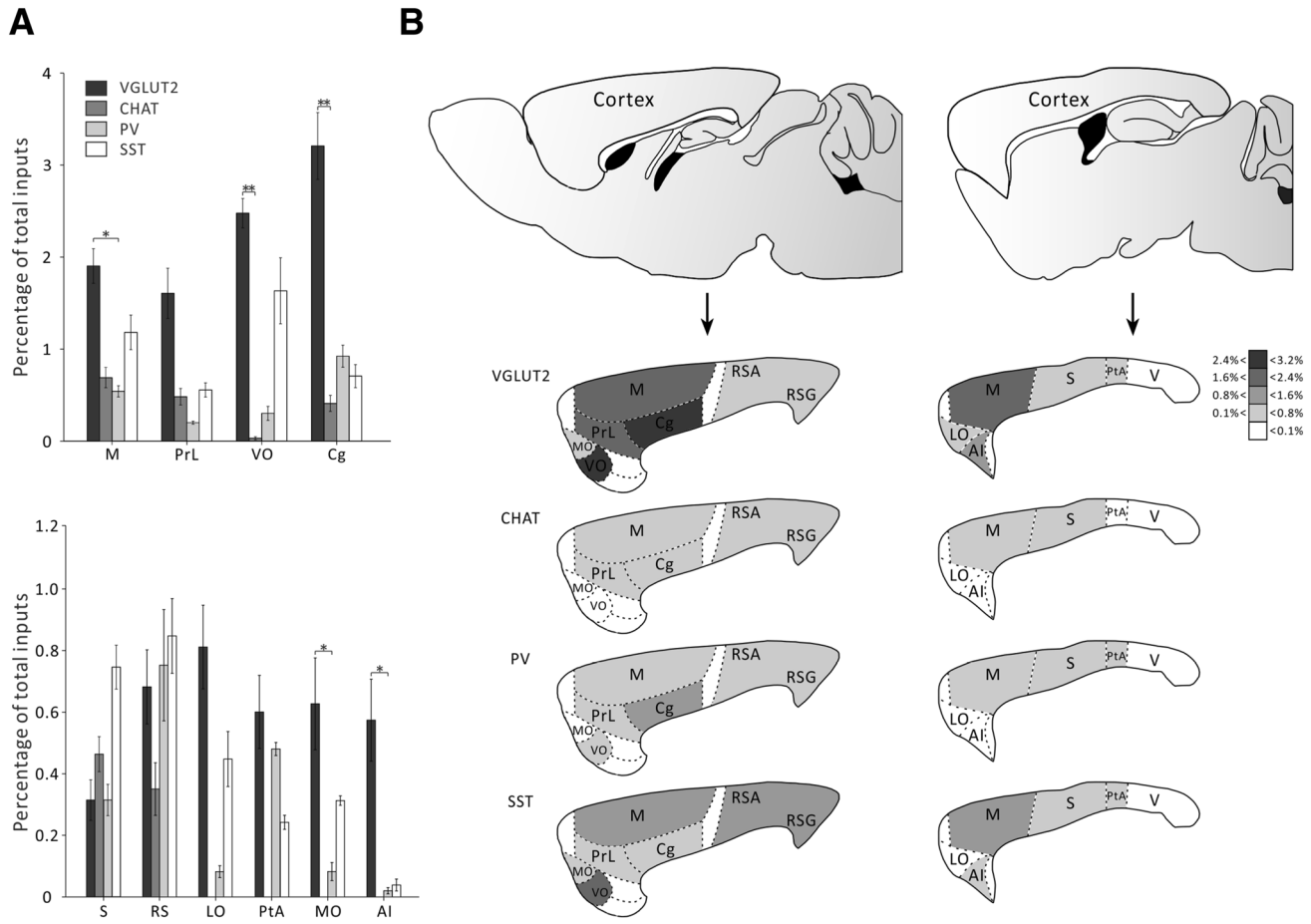

Fig. 7 Comparison of afferent intensity of different nuclei from cortex to the LDT. **A** Distribution of afferent intensity from selected cortical regions to each LDT cell type (n=4, $^*P$ <0.05, mean ± SEM). **B** Schematic of afferent intensity of selected cortical regions representing the percentages of total inputs per region for each LDT cell type.

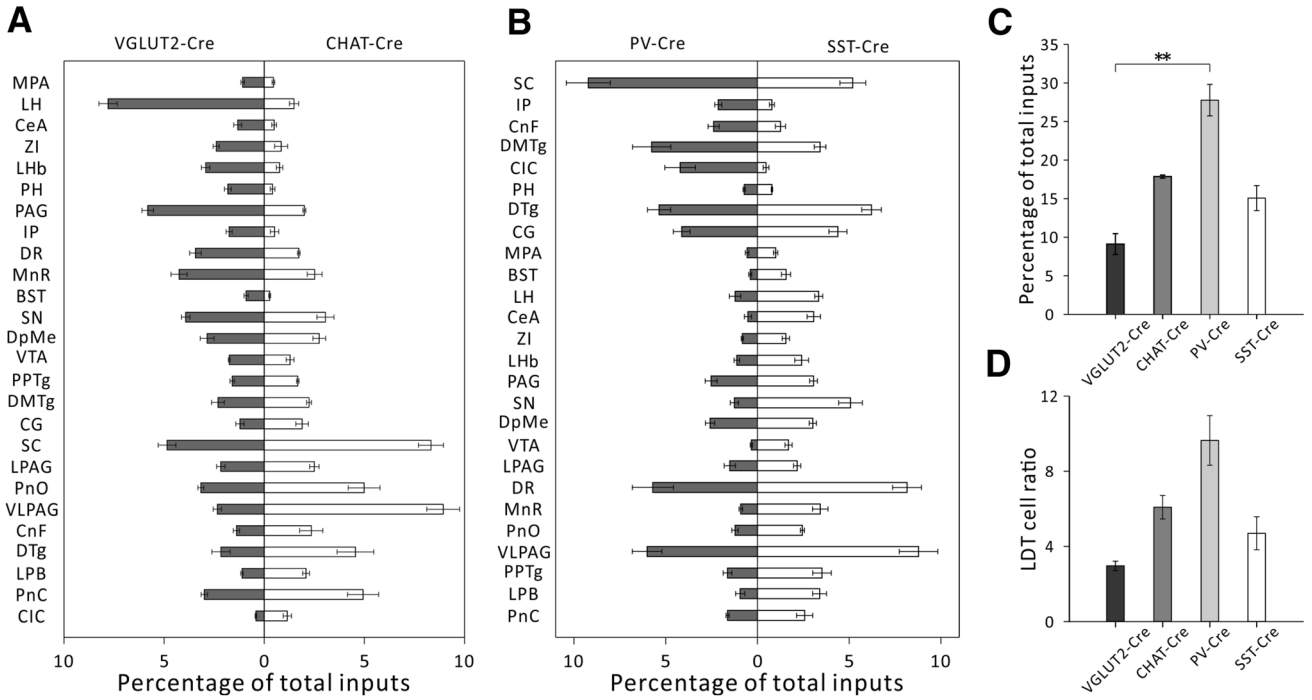

Fig. 8 Comparison of the afferent intensity of different nuclei between different cell types and the local LDT inputs to different cell types. **A** Comparison of the afferent intensity from different nuclei in VGLUT2-IRES-CRE mice and CHAT-IRES-CRE mice. **B** Comparison of the afferent intensity in PV-IRES-Cre mice and SST-IRES-Cre mice. **C** Local LDT afferent intensity in the four cell types. We used the fraction input cell counts in the LDT/whole brain input cell counts to measure the afferent intensity ($n = 4$, $^{**}P < 0.01$, mean ± SEM). **D** Ratios of all input cell counts of the LDT to starter cell counts ($n = 4$, $P = 0.092$, mean ± SEM).

this may allow the rabies virus to infect and label some cells with DsRed at the injection site. The lack of sufficient RG in these cells then prevented the trans-synaptic spread of RV [25]. This shortcoming did not affect the statistics of the long-range inputs but led to a slight overestimation of local inputs. To further explore the local inputs to different cell types within the LDT, we determined the LDT cell ratios by dividing the local upstream cell number by the number of starter cells. In this way, we found that each PV^+ GABAergic cell received a considerably higher density of LDT innervation than the other cell types, although the differences were not significant (Fig. 8D). The local inputs per cell were 6.11 ± 0.62 for cholinergic, 2.99 ± 0.25 for glutamatergic, 9.67 ± 1.32 for PV^+-GABAergic, and 4.73 ± 0.88 for SOM^+-GABAergic cells.

Discussion

Using a modified rabies virus retrograde tracing system, we identified the whole-brain distributions of long-range projections to the LDT and local connections within the LDT with cell-type specificity. Due to the limitations of earlier tracing techniques, the previous anatomical tracing studies failed to quantify the statistics of afferent intensity and did not reveal cell-type specificity. Our study also found that the LDT received direct inputs from the motor and retrosplenial cortices, which was not reported in previous studies [21, 22]. This disparity with earlier studies could be explained in that our rabies virus retrograde tracing technique may have a higher resolution. Alternatively, these differences could be due to the fact that our data were from mice, whereas previous studies used rats. One caveat of the current study is that the differences in input projection intensity could be due to the selectivity or efficiency of RV targeting. Therefore, further studies using anterograde tracing or slice electrophysiological recording techniques are required to address this issue.

Due to technical limitations, this study had a few shortcomings that may have had a small effect on the statistical results. First, after the perfusion process, as the brain was removed from the skull, it was extremely difficult to avoid damage to the olfactory bulb, and this may have affected the statistic of inputs from the bulb. Second, the viruses may have leaked into the dorsal tegmental nucleus, a nucleus near the LDT. Consequently, very few starter cells appeared in this nucleus and therefore the afferents to the LDT may have been overestimated.

It is important to note that a number of starting conditions could also affect the estimation of starter cell numbers in the LDT. For example, it is possible that some LDT cells containing TVA-eGFP may not have contained

RG due to the separation of these constructs into different vectors. When counting TVA-eGFP/RV-DsRed-positive cells as starters, this could lead to an overestimation of the number of starter cells as it was not confirmed that all of them contain RG. On the other hand, a population of starter cells might be highly interconnected among each other, which is very likely to occur in the LDT. These TVA-eGFP/RV-DsRed double-labelled cells could be either primarily or retrogradely transduced by RV. In this case, the number of starter cells would be overestimated and the number of local presynaptic cells underestimated.

According to our data, in some nuclei quantitative afferent differences began to emerge. For example, in spite of making connections with all four types of cells, the lateral habenula (LHb) preferred to target SOM^+- rather than PV^+-GABAergic neurons. Previous studies found that activation of the SOM^+ cells reduces fear. It should be anti-fear response for the activation of LHb-LDT pathway, considering that of SOM^+-GABAergic cells receive more glutamatergic LHb innervation than PV^+ GABAergic cells [7]. On the contrary, the LHb promotes fear responses through its glutamatergic projections to the LDT. In addition, although the LH sent projections to different cell types in the LDT in a similar manner and pattern to that of the LHb, optogenetic activation of the LH-LDT pathway fails to induce fear-like behavior [7]. Therefore, it is very likely that the upstream information converges on and is processed by local micro-circuitry within the LDT to produce a specific behavioral output. This speculation was supported by the fact that all LDT cell types received very strong local innervation, as showed in Fig. 8C, D.

Notably, it seems that the sensory cortical areas and the thalamus only send very sparse innervation to the LDT. This suggests that sensory cues are unlikely to be directly transmitted to the LDT. On the other hand, the cortical inputs to the LDT mostly originate from the limbic lobe, including the ventral orbital, prelimbic, and cingulate cortices, indicating that higher-order processes of cognition may evaluate the environmental stimuli related to danger or reward [26, 27], and then transmit the information to the LDT to guide the animals' behavioral outputs.

Taking all the data into consideration, the majority of the inputs to the LDT came from the midbrain, hindbrain, cortex, and hypothalamus, with quite a few belonging to the limbic system, including the LH, LHb, VTA, and central amygdala. These results together with those of previous studies [7, 19], suggest that the LDT may be a key nodal structure as an emotional center of the brain. To further understand the role of the LDT in different behaviors, such as arousal, reward, and innate fear, it will be of great interest to uncover the functional implications of the inputs from different upstream nuclei to the LDT.

Acknowledgements We thank Chris Wood for critical comments on this manuscript. This work was supported by grants from the National Natural Science Foundation of China (31671100, 31471022, 31622027, 31490592, 81527901, and 81521062), Zhejiang Provincial Natural Science Foundation, China (LR18H090001), the Program for Introducing Talents in Disciplines to Universities, and the Fundamental Research Funds for the Central Universities, China (2017YFA7002, and 2019QNA5001).

Conflict of interest The authors declare that there are no conflicts of interest.

References

1. Lodge DJ, Grace AA. The laterodorsal tegmentum is essential for burst firing of ventral tegmental area dopamine neurons. Proc Natl Acad Sci U S A 2006, 103: 5167–5172.
2. Kohlmeier KA. Off the beaten path: drug addiction and the pontine laterodorsal tegmentum. ISRN Neurosci 2013, 2013: 604847.
3. Coimbra B, Soares-Cunha C, Borges S, Vasconcelos NA, Sousa N, Rodrigues AJ. Impairments in laterodorsal tegmentum to VTA projections underlie glucocorticoid-triggered reward deficits. Elife 2017, 6.
4. Lu J, Sherman D, Devor M, Saper CB. A putative flip-flop switch for control of REM sleep. Nature 2006, 441: 589–594.
5. Sakai K. Paradoxical (rapid eye movement) sleep-on neurons in the laterodorsal pontine tegmentum in mice. Neuroscience 2015, 310: 455–471.
6. Van Dort CJ, Zachs DP, Kenny JD, Zheng S, Goldblum RR, Gelwan NA, *et al.* Optogenetic activation of cholinergic neurons in the PPT or LDT induces REM sleep. Proc Natl Acad Sci U S A 2015, 112: 584–589.
7. Yang H, Yang J, Xi W, Hao S, Luo B, He X, *et al.* Laterodorsal tegmentum interneuron subtypes oppositely regulate olfactory cue-induced innate fear. Nat Neurosci 2016, 19: 283–289.
8. Ford B, Holmes CJ, Mainville L, Jones BE. GABAergic neurons in the rat pontomesencephalic tegmentum: codistribution with cholinergic and other tegmental neurons projecting to the posterior lateral hypothalamus. J Comp Neurol 1995, 363: 177–196.
9. Wang HL, Morales M. Pedunculopontine and laterodorsal tegmental nuclei contain distinct populations of cholinergic, glutamatergic and GABAergic neurons in the rat. Eur J Neurosci 2009, 29: 340–358.
10. Armstrong DM, Saper CB, Levey AI, Wainer BH, Terry RD. Distribution of cholinergic neurons in rat brain: demonstrated by the immunocytochemical localization of choline acetyltransferase. J Comp Neurol 1983, 216: 53–68.
11. Brudzynski SM. The ascending mesolimbic cholinergic system–a specific division of the reticular activating system involved in the initiation of negative emotional states. J Mol Neurosci 2014, 53: 436–445.
12. Li X, Yu B, Sun Q, Zhang Y, Ren M, Zhang X, *et al.* Generation of a whole-brain atlas for the cholinergic system and mesoscopic projectome analysis of basal forebrain cholinergic neurons. Proc Natl Acad Sci U S A 2017.
13. Boucetta S, Cisse Y, Mainville L, Morales M, Jones BE. Discharge profiles across the sleep-waking cycle of identified cholinergic, GABAergic, and glutamatergic neurons in the pontomesencephalic tegmentum of the rat. J Neurosci 2014, 34: 4708–4727.

14. Ishibashi M, Leonard CS, Kohlmeier KA. Nicotinic activation of laterodorsal tegmental neurons: implications for addiction to nicotine. Neuropsychopharmacology 2009, 34: 2529–2547.
15. Nelson CL, Wetter JB, Milovanovic M, Wolf ME. The laterodorsal tegmentum contributes to behavioral sensitization to amphetamine. Neuroscience 2007, 146: 41–49.
16. Omelchenko N, Sesack SR. Laterodorsal tegmental projections to identified cell populations in the rat ventral tegmental area. J Comp Neurol 2005, 483: 217–235.
17. Omelchenko N, Sesack SR. Cholinergic axons in the rat ventral tegmental area synapse preferentially onto mesoaccumbens dopamine neurons. J Comp Neurol 2006, 494: 863–875.
18. Oakman SA, Faris PL, Cozzari C, Hartman BK. Characterization of the extent of pontomesencephalic cholinergic neurons' projections to the thalamus: comparison with projections to midbrain dopaminergic groups. Neuroscience 1999, 94: 529–547.
19. Lammel S, Lim BK, Ran C, Huang KW, Betley MJ, Tye KM, *et al.* Input-specific control of reward and aversion in the ventral tegmental area. Nature 2012, 491: 212–217.
20. Xiao C, Cho JR, Zhou C, Treweek JB, Chan K, McKinney SL, *et al.* Cholinergic mesopontine signals govern locomotion and reward through dissociable midbrain pathways. Neuron 2016, 90: 333–347.
21. Satoh K, Fibiger HC. Cholinergic neurons of the laterodorsal tegmental nucleus: efferent and afferent connections. J Comp Neurol 1986, 253: 277–302.
22. Cornwall J, Cooper JD, Phillipson OT. Afferent and efferent connections of the laterodorsal tegmental nucleus in the rat. Brain Res Bull 1990, 25: 271–284.
23. Wall NR, Wickersham IR, Cetin A, De La Parra M, Callaway EM. Monosynaptic circuit tracing in vivo through Cre-dependent targeting and complementation of modified rabies virus. Proc Natl Acad Sci U S A 2010, 107: 21848–21853.
24. Wickersham IR, Lyon DC, Barnard RJ, Mori T, Finke S, Conzelmann KK, *et al.* Monosynaptic restriction of transsynaptic tracing from single, genetically targeted neurons. Neuron 2007, 53: 639–647.
25. Faget L, Osakada F, Duan J, Ressler R, Johnson AB, Proudfoot JA, *et al.* Afferent inputs to neurotransmitter-defined cell types in the ventral tegmental area. Cell Rep 2016, 15: 2796–2808.
26. Zhang YY, Xu L, Liang ZY, Wang K, Hou B, Zhou Y, *et al.* Separate neural networks for gains and losses in intertemporal choice. Neurosci Bull 2018, 34: 725–735.
27. Fan L, Jiang T. Mapping underlying maturational changes in human brain. Neurosci Bull 2017, 33: 478–480.